Journal of Volcanology and Geothermal Research 391 (2020) 106351

Contents lists available at ScienceDirect

Journal of Volcanology and Geothermal Research

journal homepage: www.elsevier.com/locate/jvolgeores

Improving fluid flow in geothermal reservoirs by thermal and mechanical stimulation: The case of Krafla volcano, Iceland

G.H. Eggertsson [a,*], Y. Lavallée [a], J.E. Kendrick [a], S.H. Markússon [b]

[a] Department of Earth, Ocean and Ecological Sciences, University of Liverpool, 4 Brownlow Street, Liverpool L69 3GP, United Kingdom
[b] Landsvirkjun, Háaleitisbraut 68, 110 Reykjavík, Iceland

ARTICLE INFO

Article history:
Received 3 November 2017
Received in revised form 22 February 2018
Accepted 9 April 2018
Available online 11 April 2018

ABSTRACT

The magmatic-hydrothermal system at Krafla Volcano, North-East Iceland, is an important source of fluids exploited for geothermal energy. Here, we employ laboratory measurements to constrain the porosity and permeability of the main lithologies forming the reservoir, and investigate the impacts of different thermal and mechanical stimulation practices to improve fluid flow.

Six main rock types were identified and sampled: three basalts (a dense and a porous lava, and a surficial dyke); a hyaloclastite; an obsidian; an ignimbrite; a felsite; and a gabbro. Permeability measurements were made in a hydrostatic cell using the steady-state flow method at a range of confining pressures (1–100 MPa). The measurements show that permeability generally increases with porosity, but that permeability may vary significantly for a given porosity, depending on the presence of pore connectivity and micro-fractures. We note that an increase in effective pressure results in a decrease in permeability due to closure of pre-existing cracks, abundant in some rocks. When unloading, samples fail to recover pre-loading permeability, as cracks do not necessarily entirely reopen. To further examine the hysteresis imposed by crack closure, we cyclically loaded/unloaded a felsite sample ten times by varying pore pressure which resulted in a further nonlinear decreases in permeability with each pressurisation cycle; thus an understanding of the pressurisation path may be a requirement to constrain fluid flow variations in geothermal systems.

To test the effects of thermal stimulation on fluid flow, samples of dense basalt and felsite were thermally stressed by heating to 450 °C and cooling at different rates (in air, in water and at a controlled rate of <5 °C·min^{-1}). The results show that the permeability of originally highly fractured rocks is not affected by thermal stressing, but originally unfractured rocks show a nonlinear increase in permeability with each thermal stressing cycle, especially with the largest thermal shock imposed by quenching in water; thus thermal stimulation may not be expected to result in a similar magnitude of permeability creation along the length of a borehole.

Finally, following the permeability measurements on intact rocks, the Brazilian tensile testing method was employed to impart one and two (orthogonal) macro-fractures, and permeability was measured after each step. The creation of one macro-fracture strongly enhanced the permeability of the rock (especially dense rocks), resulting in a narrower range of permeability (as a function of porosity) for the fractured rocks. Imparting a second fracture had trivial additional impact on the permeability of the rock. Yet, the presence of fine fragments and possible minor offset of fracture interfaces was found to obstruct fracture closure, which resulted in higher permeability irrespective of effective pressure; thus hydraulic fracturing may locally increase fluid flow, especially when employing proppants to obstruct fracture closure and ensure a stable permeable network in a reservoir.

We discuss the implications of the findings for a first order constraint on the permeability of the reservoir rock and the potential of thermal and mechanical stimulation methods on energy production in geothermal systems nested in active volcanic fields.

1. Introduction

1.1. Fluid flow in reservoirs

Fluid flow in geomaterials has been the subject of numerous studies since the pioneering efforts of Henry Darcy (Darcy, 1856; Darcy, 1857).

* Corresponding author.
E-mail address: g.eggertsson@liverpool.ac.uk (G.H. Eggertsson).

https://doi.org/10.1016/j.jvolgeores.2018.04.008

These studies have highlighted the central importance of fluid flow in many environments, namely: water aquifers (e.g. Strehlow et al., 2015), petroleum and gas reservoirs (e.g. Jansen, 2011), volcanoes (e.g. Edmonds and Herd, 2007), and hydrothermal systems utilised for geothermal energy (e.g. Darling and Armannsson, 1989) – the subject of this study.

Hydrothermal systems are widespread on Earth and whilst they have been utilised for their thermal output in many cultures (e.g. Carlino et al., 2012; Gallois, 2007), they have long been recognised to be a source of devastating volcanic hazards (e.g. Gudmundsson et al., 2008; Hansell and Oppenheimer, 2004). Within active hydrothermal systems, the porous and fracture networks of the reservoir rocks may store high-pressure and temperature fluids that can be extracted for geothermal energy production (Gudmundsson, 1995) – a procedure established in 1904 by Italian scientist Piero Ginori Conti (Tiwari and Ghosal, 2005), and increasingly practiced in our efforts to deliver clean, renewable energy. The storage capacity of a reservoir is directly related to the porosity of the rock and the compressibility of the fluids (dependent on their chemistry), and our ability to extract these fluids requires a high degree of pore connectivity (e.g. Siratovich et al., 2014). Hence, permeability within exploited geothermal fields has an important control on both productivity and the sustainability of fluid flow within the reservoir. The development of permeability (whether natural or anthropogenic) has a great impact on the success, magnitude, and sustainability of energy production (Mock et al., 1997; Zimmermann et al., 2009).

The architecture of the porous network of rocks and, as a result permeability, varies widely in nature (e.g. Ashwell et al., 2015; Brace, 1980; Cant et al., 2018; Eichelberger et al., 1986; Farquharson et al., 2015; Heap et al., 2014a; Heap and Kennedy, 2016; Heap et al., 2014b; Heap et al., 2016; Jouniaux et al., 2000; Kendrick et al., 2016; Kendrick et al., 2013; Klug and Cashman, 1996; Kushnir et al., 2016; Lamur et al., 2017a; Mueller et al., 2005; Okumura and Sasaki, 2014; Saar and Manga, 1999; Schaefer et al., 2015; Stimac et al., 2004). This is especially the case for volcanic rocks, as they have undergone complex petrogenetic and deformation histories during their formation (Farquharson et al., 2015; Kendrick et al., 2013; Klug and Cashman, 1996; Schaefer et al., 2015). For instance, during explosions, the pores which store the gas that triggers fragmentation are frozen into the lavas as they erupt; in contrast, the pore geometry of effusive lavas reflect a complex history of deformation, which results from bubble growth, coalescence, collapse and fracturing. Dense volcanic rocks are generally found to contain flattened and/or irregular (concave) pores and multiple micro-fractures, whereas highly vesicular volcanic rocks tend to have sub-rounded (convex) pores. As a result, explosive products have been described to hold a different permeability-porosity relationship than effusive products (Mueller et al., 2005). In addition, it has been suggested that there is a porosity change point (14–20%) in microstructural control on effusive volcanic rock permeability, due to changes in relative tortuosity and pore throat size of the variably constructed porous networks of dense and porous rocks (Farquharson et al., 2015).

At depth, volcanic rocks may have different properties. Volcanic rocks buried by subsequent eruptive products – as is commonly the case in caldera systems (the setting of the geothermal system in this study) – tend to compact, closing micro-fractures (Kolzenburg et al., 2012), and if stress is sufficient, deformation may modify the architecture of the porous network (e.g. Heap et al., 2015a). Both micro-fracture closure (e.g. Lamur et al., 2017a; Tanikawa and Shimamoto, 2009) and shear-enhanced compaction (Heap et al., 2015a) generally decrease the permeability of rocks buried at depth. When directly emplaced in the crust, intrusive volcanics tend to have low contents of vesicles and micro-fractures, and their permeability is equally low (Murphy et al., 1981), at least, at a small scale (Brace et al., 1968); yet, at a large scale, cooling contraction can trigger the development of columnar joints (Degraff and Aydin, 1993; Kantha, 1981), providing preferential fluid pathways (Lamur et al., 2018).

Geothermal exploitation relies heavily on the presence of fractures to optimise fluid flow and energy generation. During drilling operations, a number of methods have been applied to enhance the extent of permeable fractures (e.g. Aqui and Zarrouk, 2011), whether through hydraulic fracturing (e.g. Legarth et al., 2005; McClure and Horne, 2014; Miller, 2015; Murphy et al., 1981; Tomac and Gutierrez, 2017; Zang et al., 2014; Zimmermann et al., 2011) or thermal stimulation (e.g. Grant et al., 2013; Siratovich et al., 2015b). In high-temperature, high-enthalpy geothermal reservoirs, where the rock may exhibit ductile behaviour (e.g. Violay et al., 2012), it is commonly presumed that fractures would not remain opened nor preferentially oriented for long periods of time (e.g. Scott et al., 2015). This may be the case if temperature is sufficient, such that the diffusivity of the main rock forming minerals and melt (if present), favours fracture healing (e.g. Farquharson et al., 2017; Lamur et al., 2017b; Tuffen et al., 2003) or viscous deformation of the porous network (Kendrick et al., 2013; Kushnir et al., 2017b). However, such rapid closure of permeability can be overcome if the rock remains fractured by keeping stress sufficiently high (e.g. Lavallée et al., 2013), by building pore overpressure (e.g. Pearson, 1981) or by keeping temperature low (Lavallée et al., 2008), thus thermally contracting the rock (e.g. Siratovich et al., 2015b). Understanding the permeability of reservoir rocks, the sustainability of conditions and the longevity of production is key to characterising the potential exploitability of hydrothermal reservoirs for geothermal energy. Laboratory experimentation can help provide necessary constraints for material behaviour in simulated geothermal reservoir conditions (Ghassemi, 2012). For example, the presence of macroscopic fractures may significantly increase the permeability of rocks, especially of dense rocks (Eggertsson et al., 2016; Heap and Kennedy, 2016; Heap et al., 2015b; Lamur et al., 2017a; Nara et al., 2012).

1.2. Geological setting of the Krafla geothermal system

Krafla is a caldera volcano, located in North-East Iceland (Fig. 1a). The volcanic field hosts a partly filled caldera of about 8 × 10 km (Sæmundsson, 1991; Fig. 1b) and is intersected by a 90 km long fissure swarm trending NNE (Hjartardottir et al., 2012). The caldera hosts an active hydrothermal system, approximately 10 km^2 in size. In the Holocene, fissure eruptions recurring every 300–1000 years characterised the volcanic activity (Sæmundsson, 1991). In 1724, the Myvatn fires occurred west of Krafla; this coincided with a 5-year explosive phreatomagmatic eruption at Viti, which exposed at the surface gabbroic and felsitic lithics originating at depth in the system. The most recent eruption was the Krafla fires, which initiated in 1975 and resulted in the outpouring of basaltic lava for 9 years (Einarsson, 1991). Magmatic activity associated with the eruption impacted the chemical composition of the fluids within the reservoir (Guðmundsson, 2001; Ármannsson, 1989) and led to increased hydrothermal activity (Einarsson, 1978; Einarsson, 1991; Sæmundsson, 1991).

In 1974, the government of Iceland initiated the construction of a geothermal power plant within the caldera. The aim was to install two turbines to produce 60 MW_e, but due to problems associated with the Krafla fires eruption, the power plant only used one turbine until 1999; now that both turbines operate, the power plant readily produces 60 MW_e (Guðmundsson, 2001). In 2009 the Krafla geothermal field became site of the Iceland deep drilling project (IDDP-1), with the aim to source deep, high-enthalpy, supercritical geothermal fluids at a depth of 4–5 km (Fridleifsson et al., 2014). This attempt terminated abruptly as the drill string penetrated an active rhyolitic magma body at a depth of 2.1 km (Elders et al., 2014). During flow tests of this, the World's hottest producing geothermal well, near-magmatic fluid entering the well head at a temperature exceeding 450 °C resulted in the transport of dry superheated steam at high pressures (40–140 bar), which due to its corrosive nature severely damaged the equipment and production ceased soon thereafter (Elders et al., 2014). Yet, this unique opportunity demonstrated the possibility of producing 35 MW_e from a single well

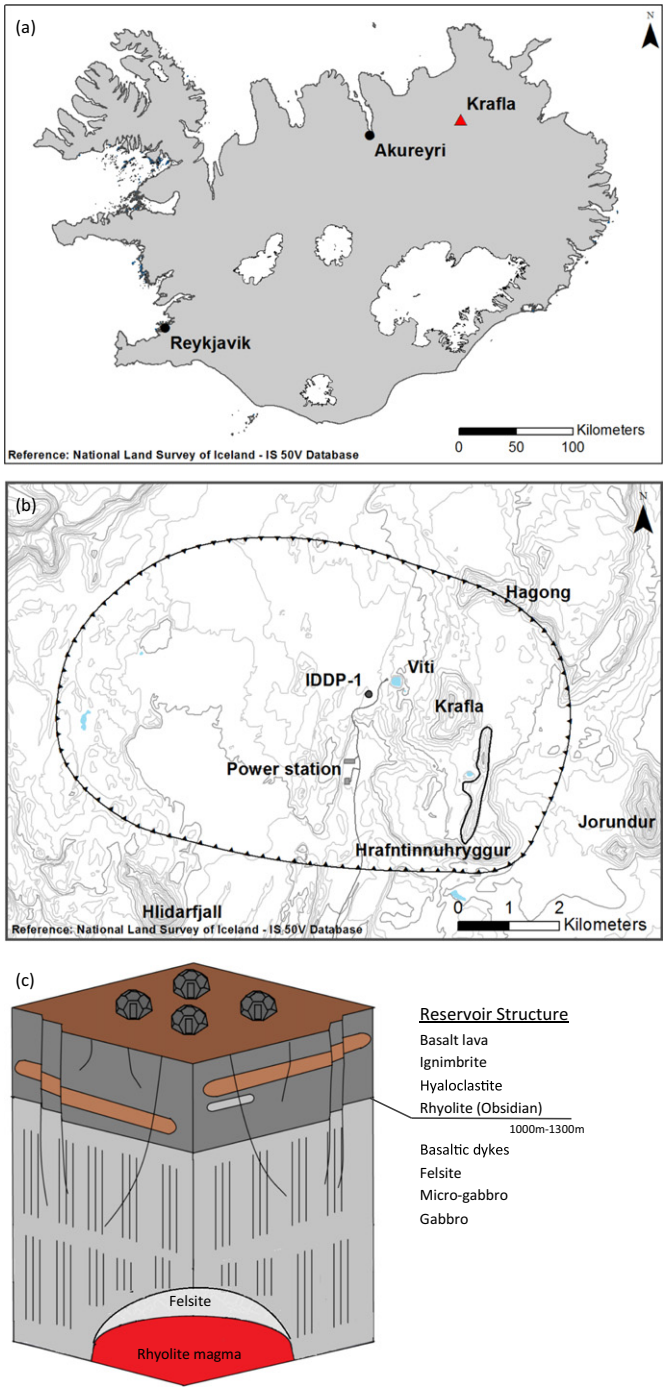

Fig. 1. (a) Location of the Krafla volcanic field in North-East Iceland. (b) Overview of the Krafla caldera, delimited by the line with tic marks (after Sæmundsson, 1991). The map shows the location of key features, in particular the power station, the Viti crater, the drill site of IDDP-1 and Hraftinnuhryggur (a large obsidian ridge). (c) Schematic of the lithologies comprising the Krafla geothermal reservoir. The uppermost 1000–1300 m of the reservoir are primarily made up of extrusive rocks, including lavas, ignimbrite and hyaloclastite. At greater depth, the reservoir is dominated by intrusive volcanics, gabbro and felsite (Mortensen et al., 2015). In a part of the system, rhyolitic magma was encountered at a depth of 2.1 km (Elders et al., 2014).

(Ingason et al., 2014), and helped define parts of the geothermal system for the first time, constraining the pressure (Elders et al., 2011) and temperature (Axelsson et al., 2014; Elders et al., 2011) conditions in the encountered rhyolite body. Volatile concentrations measured in glass shards recovered during drilling in magma were used to define a pressure of ~30–50 MPa (Zierenberg et al., 2013), which is lower than that expected from lithostatic pressure (ca. 50–70 MPa; considering a depth of 2.1 km and assuming a range of rock densities between 2.5–3.3 kg·m^{-3}), but above hydrostatic pressure (~21 MPa) for this depth (Elders et al., 2011). This pressure discrepancy suggests that fluid pressure at the encountered magma body may be affected by connectivity across the hydrothermal system (e.g. Fournier, 1999).

Examination of drilling products (cores and cuttings) has provided a view of the rocks and structures hosting the reservoir fluids in the Krafla geothermal system. The observations suggest that the upper 1000–1300 m of the reservoir, where temperatures are ca. 100–300 °C, primarily consists of variably indurated and welded ignimbrite, intact as well as fractured basaltic lavas and variably compacted hyaloclastite. At depths below 1000–1300 m, where temperature may reach ca. 350 °C, the reservoir is made up of intrusive volcanics, primarily gabbro and felsite, which both show variable degrees of fracture damage (Bodvarsson et al., 1984; Mortensen et al., 2014; Sæmundsson, 1991). The last rock encountered before reaching the near aphyric magma body during IDDP-1 was a felsite sill (argued to be the crystallised, mushy, magmatic aureole) which totalled ~80 m in thickness (Mortensen et al., 2014). This magmatic aureole is characterised by a sharp temperature increase from ~400 to ~900 °C (e.g., Mortensen et al., 2014; Axelsson et al., 2014; Elders et al., 2014). Thus, 40 years of extensive drilling operations in and around the Krafla caldera has provided us with invaluable information that helped reconstruct the reservoir rock (Fig. 1c). This study aims to constrain the permeability of these rocks, and assess how different thermal and mechanical stimulation methods may improve fluid flow in the hydrothermal system, and ultimately inform decisions to improve geothermal productivity in high-enthalpy systems.

2. Materials and Methods

2.1. Rock samples

During a field survey in Autumn 2015, and through information gathered from previous drilling exercises, six main rock types were identified and sampled to carry out this study (see Supplementary Data): three basalts (a lava with 11 to 27% porosity, a basalt dyke with 31–36% porosity, and a porous lava with 34 to 60% porosity); one hyaloclastite (35–45% porosity); one obsidian (1–5% porosity); one ignimbrite (14–17% porosity); one felsite (9–18% porosity) and one gabbro (11–15% porosity). The samples host a spectrum of pore microstructures (Fig. 2), which we anticipated would result in equally diverse permeability properties. The samples were loose blocks (therefore not orientated), collected from surface outcrops without hammering to prevent adding fracture damage and compromising the porosity and permeability values determined here; the felsite and microgabbros (which form the roof of the magma reservoir; Mortensen et al., 2014) were erupted explosively through, and scattered around, Víti crater during the Mývatn fires (Sæmundsson, 1991).

2.2. Experimental methods

Here, we aim to constrain the natural range of permeability of reservoir rocks and investigate how to enhance fluid flow by testing the effects of thermal and mechanical stimulation methods; including the impact of pressure oscillations, thermal stressing and fracturing. This was done in several steps: first, we measured the porosity and permeability of all rock samples as collected; second, we subjected them to the thermal or mechanical stimulation methods (see below); and finally, we measured the permeability anew.

In this study over 120 core samples were prepared from large blocks of the aforementioned six rock types, and tested to constrain the range of porosity and permeability of each: As loose samples of blocks were collected from outcrops with no strong fabrics, cores were prepared in no particular orientation, yet parallel to one another within a given block. To examine the influence of a macro-fracture on the permeability

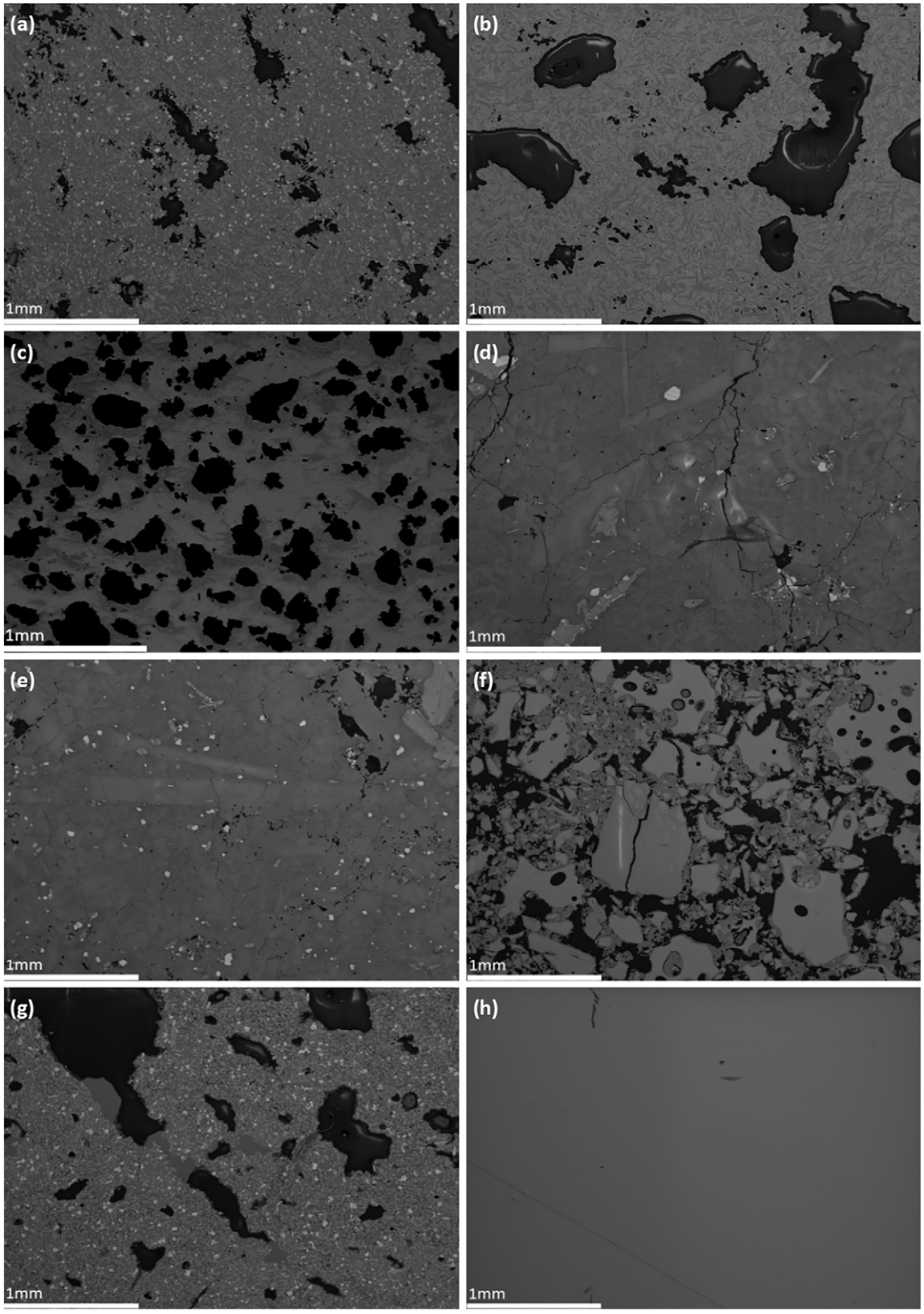

Fig. 2. Backscattered electron (BSE) images (obtained by scanning electron microscope (SEM)) of the main Krafla reservoir lithologies. (a) Microcrystalline basalt with 11% porosity, consisting of irregular vesicles with a range of sizes (<1 mm), tortuosity and connectivity; micro-fractures are sparsely present but too narrow to be visible at this scale. (b) Microcrystalline basalt with 45% porosity, comprising a bimodal porous network made of large and generally rounded, though slightly irregular, vesicles (<2 mm) and small irregularly-distributed vesicles; micro-fractures are sparsely present but too narrow to be visible at this scale. (c) Basalt dyke sample with 32% porosity, predominantly made of relatively evenly-distributed, sub-rounded vesicles (100–400 μm); the rock contains a trivial amount of very narrow micro-fractures. (d) Felsite with 11.5% porosity, consisting of very few small and irregular vesicles, sometimes connected by micro-fractures, up to 10–20 μm wide. (e) Gabbro with 12% porosity, made up of a connected network of many small, irregular-shape vesicles, and poorly-developed micro-fractures. (f) Hyaloclastite with 40% porosity, made up of irregular-shape pores between a highly fragmental, angular glass and crystalline assemblage. Micro-fractures as wide as 20 μm are visible in larger fragments. (g) Ignimbrite with 15% porosity, comprising generally elongate and sub-rounded vesicles, and a lack of micro-fractures visible at any scale. (h) Dense obsidian with scarce micro-vesicles (<0.01%) and no obvious micro-fractures.

of rocks core samples with a diameter of 26 mm and a thickness of ~13 mm were prepared; to investigate the impact of pressure fluctuations on permeability, cylindrical samples of felsite with a diameter and thickness of 26 mm were tested; for the investigation of thermal stressing impact on permeability, cylindrical samples of felsite and basalt with diameter of 25 mm and length of 50 mm were prepared and tested. The samples were kept in a drying oven at 75 °C after preparation, then left to cool in a desiccator before determinations of the porosity and permeability. The permeability dataset, obtained through the above experimental program, was complemented by additional porosity/permeability measurements on 50 mm long by 25 mm diameter core samples (see Supplementary Data), which will be used in a future mechanical study of Krafla rocks (Eggertsson et al., in preparation).

2.2.1. Porosity and Permeability

The connected porosity of the cores was determined using an AccuPyc 1340 Helium pycnometer from Micromeritics. The device measures the sample skeletal volume (i.e., the volume of the solid rock as well as isolated pores which cannot be accessed by helium gas) in chambers of 100 cm^3 and 35 cm^3 (depending on the size of the sample), which provides a volume determination accuracy for the sample of ± 0.1%. The measurement, together with the sample weight, constrains the relative sample density (including isolated pore space), and as we know the volume of the initial sample core, we can determine the fraction of connected pores.

The permeability of the cores was measured in a hydrostatic pressure cell from Sanchez Technologies (Fig. 3a) using the steady-state flow method. A water-saturated core was placed inside a rubber jacket and loaded in the pressure vessel, making sure that the pore pressure line was water saturated. The sample assembly was then slowly pressurised using silicon oil to the desired confining pressures (5–100 MPa), spanning the conditions of the Krafla geothermal reservoir. As the sample was pressurised, the volume of water displaced by the sample compaction was monitored with a volumometer to track changes in the porosity (from the original porosity, measured by He-pycnometry) of the sample at various confining pressure. [The accuracy of the volumometer on the two Stigma 300 pumps (from Sanchez Technologies; now Core Lab) is 0.002 ml, which, when measuring fluid volume for the smallest sample volume of 6.9 cm^3, results in an accuracy of porosity determination of 0.05%.] Once equilibrated at the first confining pressure increment (e.g., 5 MPa) the rock permeability was measured using water, by imposing a pore pressure gradient of 1.5 MPa across the sample (2 MPa upstream and 0.5 MPa downstream) at an average pore pressure of 1.25 MPa, and by monitoring the flow rate at the sample exit; the permeability was only determined when the flow rate had stabilised. To assess the need for the use of Klinkenberg or Forchheimer corrections, the flow rate was varied by changing the pressure gradient and to check whether obtained permeability values changed; for the pressure gradient of interest, no such corrections were needed here. Once the permeability measurement was completed (after 20 to 600 min), the confining pressure was increased to the next increment (e.g., 10 MPa), whilst monitoring pore volume changes [generally, the pore volume decrease would stabilise (within resolution of the volumometer) after 1–10 min]; then the permeability was measured anew.

To further constrain the elastic limits of the weak, porous hyaloclastite, we constrained the effective pressure threshold for inelastic, destructive compaction (defined as P* of the rock), beyond which, an accelerated, irrecoverable compaction occurs (Zhang et al., 1990). This was done by loading a water-saturated sample in the permeameter. The confining pressure and pore pressure were increased slowly (to keep the effective pressure below 5 MPa) to 53 and 50 MPa, respectively. Then, the pore pressure was reduced (and thus the effective pressure was increased) at a rate of 0.1 MPa·min^{-1} and the volume of water within the sample was monitored. P* was defined as point of negative inflection following a linear decrease in pore volume during effective pressure loading.

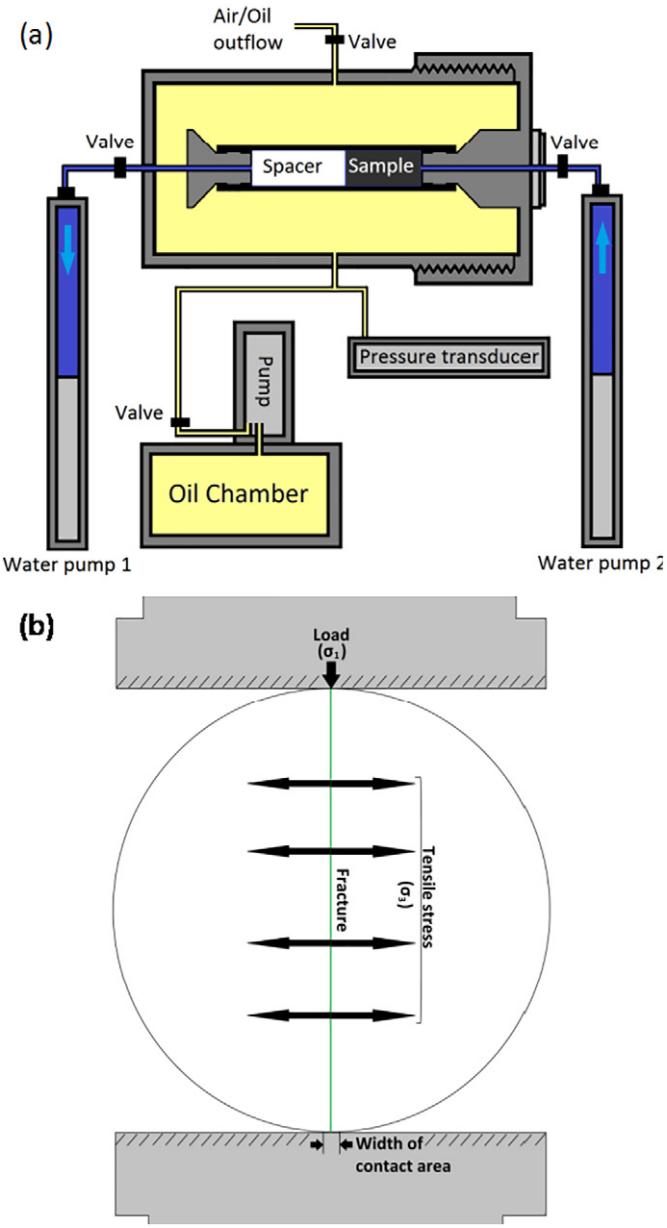

Fig. 3. (a) Schematic of the setup (hydrostatic cell and pumps) used to determine the permeability of rocks. The permeability was measured using water (injected through the sample from pump 2 to pump 1) by imposing a pressure gradient of 1.5 MPa across the sample at an average pore pressure of 1.25 MPa (upstream: 2 MPa; downstream: 0.5 MPa) for a range of confining pressures (5–100 MPa) exerted by silicon oil pumped from the oil chamber using a booster. (b) Illustration of the sample assembly to determine the tensile strength using the indirect Brazilian testing method. Here, a disc of 2:1 ratio (26 mm diameter by 13 mm thickness) is diametrically loaded at a constant displacement rate of 3 μm·s^{-1} between the pistons of an Instron press, and the load is continuously recorded.

2.2.2. Pressure fluctuations

We tested the effects of pore pressure fluctuations over 10 cycles, whilst keeping the confining pressure constant to simulate the impact of well pressure fluctuations associated with water injection during drilling operations. This was performed on felsite samples which we loaded to 39.5 MPa confining pressure and 1.5 MPa pore pressure (=38 MPa effective pressure, assuming a simple effective pressure law). An effective pressure of 38 MPa may be representative of conditions at ca. 2 km depth, near the hydrothermal-magmatic system interface (Mortensen et al., 2015). We then measured the permeability at these conditions by imposing a pressure gradient of 1 MPa across the sample

(2 MPa upstream and 1 MPa downstream). Once the permeability was measured, the pore pressure was increased to 3.5 MPa and the permeability was measured by applying a pressure gradient of 1 MPa (4 MPa upstream and 3 MPa downstream). When the permeability had been measured at the lower effective pressure (higher pore pressure), the pore pressure was lowered back down to 1.5 MPa and the same procedure repeated, in total 9 times. The effective pressure change between each stage was therefore 1.5 MPa (from 38 MPa to 36.5 MPa effective pressure and back).

2.2.3. Thermal stimulation

The impact of thermal stimulation was tested on the samples of basalt (10.9–12.1% porosity) and felsite (9.4–10.3% porosity). The porosity and permeability of 3 cores of each sample was first measured as discussed above. The samples were then heated to 450 °C at 5 °C/min in a box furnace and left for 1 h to dwell. After that, one sample of each rock type was cooled in a furnace, with a set cooling rate of 5 $°C \cdot min^{-1}$; one sample of each rock was removed from the furnace and left to cool at ambient conditions on a benchtop; and finally, one sample of each rock type was removed from the furnace and quenched in a water-filled bucket at ambient temperature. Once cooled (estimated to be sufficient to cool the whole sample after 30 min – 12 h, depending on the cooling method), the samples were then dried and their porosity and permeability were measured again. This procedure was repeated and the porosity and permeability were measured again after five and fifteen cycles. The cooling rates were chosen to represent different cooling rates experienced at different distances from boreholes during drilling activities and thermal stimulation procedures.

2.2.4. Fracturing

To induce a radial macro-fracture through the samples, the Brazilian tensile testing method was employed (Fig. 3b). A cylindrical sample was loaded diametrically in a 5969 Instron uniaxial press at a displacement rate of 3 $\mu m \cdot s^{-1}$ until a through-going fracture was produced. To ensure that the samples would not disintegrate during indirect tensile fracturing, the samples were carefully wrapped in electrical tape around the circumference (thus the mechanical data are not of publishable quality). After sample failure, the tape was carefully removed and the sample loaded into the pressure vessel for another series of permeability determinations.

For six basalt samples, a second set of fractures was then imparted, perpendicular to the first fracture in the samples. This time, however, the sample was left in the rubber jacket during loading in the press to ensure coherence. After sample failure, the permeability was measured once again under the same range of conditions as detailed above.

3. Results

3.1. Storage capacity of intact rocks

The porosity of a rock is a measure of the storage capacity for fluids and varies as a function of effective pressure (Wong and Baud, 2012). Here, we combine He-pycnometry measurements at atmospheric pressure (i.e., effective pressure of 0 MPa) and fluid volume changes measured by the volumometer in each pump during pressurisation and depressurisation in the hydrostatic pressure vessel, to constrain the evolution of porosity upon confinement.

The lithologies tested exhibit a wide range of porosities; especially the three basalt samples, which contain between 11 and 60 vol% porosity. The porosity evolution as a function of effective pressure could only be measured for four rock types (Fig. 4), as the obsidian and the ignimbrite had permeabilities too low to be determined using our setup in its current configuration (which cannot accurately constrain permeability lower than ~10^{-18} m^2). In all cases, the samples show a nonlinear decrease in pore volume with effective pressure. We note that the spread of porosity within each sample set is not particularly sensitive to

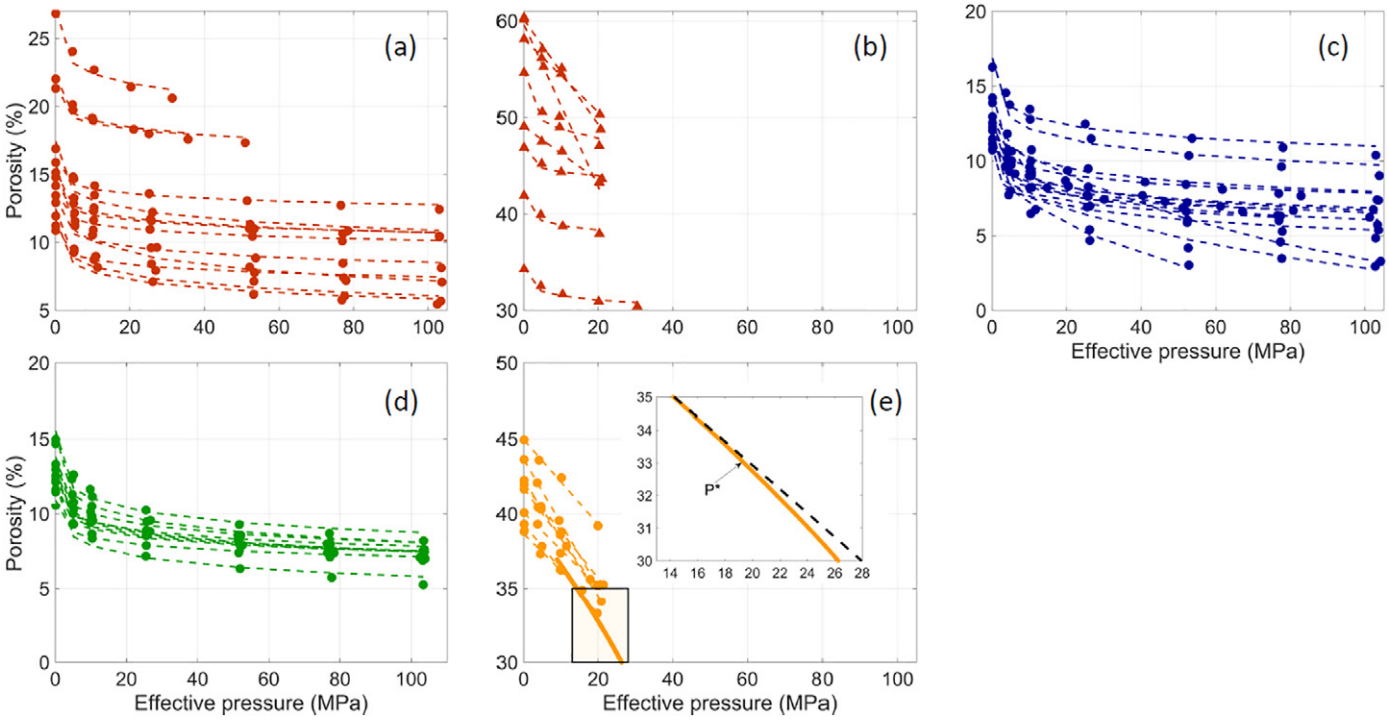

Fig. 4. Porosity evolution with effective pressure for intact (a) dense basalt (shown in Fig. 2a; 10 samples tested), (b) porous basalt (shown in Fig. 2b; 6 samples), (c) felsite (14 samples), (d) gabbro (10 samples), and (e) hyaloclastite (8 samples) as a function of effective pressure. Here, the initial porosity measurement is made by He-pycnometry, with subsequent measurements extrapolated by monitoring volume gain in the pumps (hence volume loss in the samples) during permeability measurements. The figure shows a nonlinear decrease in porosity with effective pressure, indicative of micro-fracture closure. Across the lithologies, porosity decreases most rapidly as effective pressure is increased up to ~10 MPa. Note that the scale of each graph differs. The inset in (e) shows the inelastic (destructive) compaction beyond P^*, where the rock strength is not sufficient withhold the increased pressure and starts to collapse.

effective pressure, suggesting that the nonlinear decrease in porosity with effective pressure is similar for a given rock type. For the most porous samples, the porosity decrease is slightly more pronounced (Fig. 4b, e), which may be accentuated if the effective pressure exceeds P*, resulting in crushing of the rock and compaction (e.g., hyaloclastite; inset Fig. 4e).

3.2. Permeability of intact rocks

The permeability of rocks varies as a function of porosity (e.g., Mueller et al., 2005), fracture density (e.g. Heap and Kennedy, 2016; Koudina et al., 1998) and effective pressure (e.g. Alam et al., 2014; Walsh, 1981). Here, we present permeability measurements on 60 intact samples; the basalt (1.9×10^{-16} m^2–2.5×10^{-13} m^2), felsite (1.8×10^{-15} m^2–1.1×10^{-13} m^2), gabbro (7.2×10^{-16} m^2–1.0×10^{-14} m^2) and hyaloclastite (6.0×10^{-14} m^2–1.8×10^{-13} m^2) samples show a range of permeabilities (Fig. 5). The data show that sample length (used here) has no effect on the permeability of a rock (see Supplementary Data). The basalts displayed the widest range of permeabilities (Fig. 5: 5a, b), as might be expected from their variable initial porosities (Figs. 2a–c, 4a, b). [Note that the basalt dyke was not measured under such conditions.] The densest basalt shows little change in permeability with increased pressure (Fig. 5a). The basalt samples with the highest porosities (>34 vol% porosity; Fig. 5b) show a small decrease of permeability with confining pressure (up to 20–25 MPa); lower than may be anticipated due to the porosity decrease witnessed upon pressurisation (Fig. 4b). The felsite and gabbro samples exhibit relatively larger decreases in permeability (Fig. 5c, d) in response to effective pressure than the basalts (Fig. 5a), owing to the highly fractured nature of these rocks. Yet, despite a fragmental origin of the hyaloclastite (Fig. 5e), it only exhibited moderate decrease in permeability within the low effective pressure range tested (before the samples could not sustain the effective pressure); however, the samples compacted inelastically above an effective pressure of 18 MPa (inset Fig. 4e), which resulted in a significantly lower permeability.

3.3. Impact of pressure fluctuations

During a well operation, changes in pore pressure are inevitable, from injection during drilling to functional operation at different pressures. These changes can be considered minor, but their resulting influence on the rock permeability remains poorly tested. Here, we investigate the impact on the permeability of pressurising and depressurising highly fractured felsite samples. When decreasing the pore pressure applied to a sample (at a set confinement), we note a slight increase in the rock porosity and permeability (Fig. 6a); yet, not as significant as the magnitude of porosity and permeability decrease monitored during pressurisation. Thus, pressurisation and depressurisation of porous rocks leads to hysteresis of its permeable structure on the timescales investigated here.

The hysteresis of a rock porous structure to pressure fluctuations were investigated further by testing the impact of 10 pressurisation/depressurisation cycles on the felsite by first pressurising the sample to the target confining pressure of 38 MPa (left for 30 min to equilibrate each time the pressure was changed), and fluctuating the pore pressure by 1.5 MPa (Fig. 6b). Interestingly, we note that each pressurisation cycle decreases the permeability of the rocks, which never fully recover during depressurisation (Fig. 6b). The impact is most pronounced in the first few cycles, but persists throughout all 10 cycles.

3.4. Impact of thermal stimulation

During well drilling and operation, the reservoir temperature fluctuates. To test the effect of temperature changes, we subjected felsite and basalt to thermal stress cycles by cooling from 450 °C to ambient temperature by cooling in a furnace (under controlled conditions), in air (on a benchtop) as well as in water (at ambient temperature, to quench). The data shows that the porosity and permeability of the felsite was not affected by thermal stressing, even after fifteen heating/cooling cycles (Table 1; Fig. 7). On the other hand, the porosity of the basalt was relatively unchanged (Table 1), whilst the permeability of the basalt increased by over one order of magnitude after the first five cycles; the most drastic impact being imposed by quenching in water (Fig. 7).

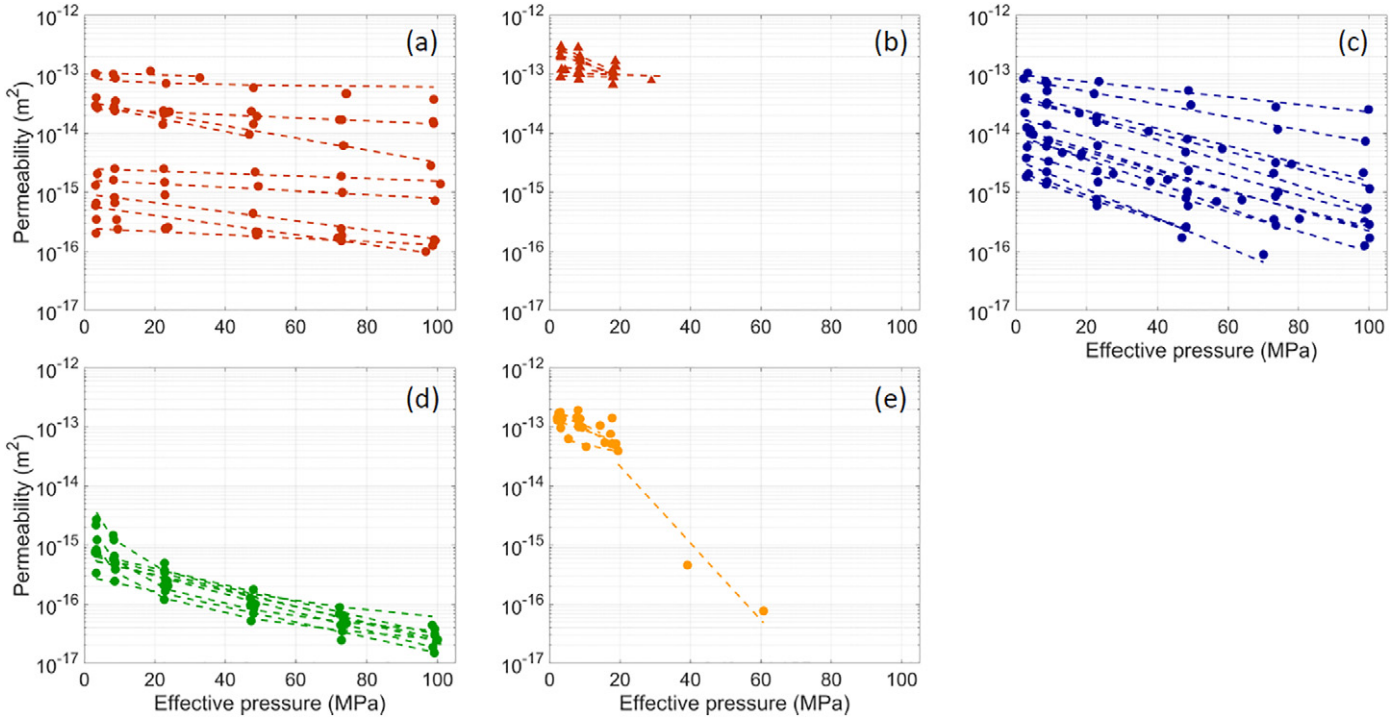

Fig. 5. Intact rock permeability evolution with effective pressure of (a) dense basalt (10 samples tested), (b) porous basalt (6 samples), (c) felsite (14 samples tested), (d) gabbro (10 samples tested), and (e) hyaloclastite (8 samples tested). The general nonlinear decrease in permeability with effective pressure is attributed to the compaction and closure of microfractures as observed by the porosity volume decrease in Fig. 4.

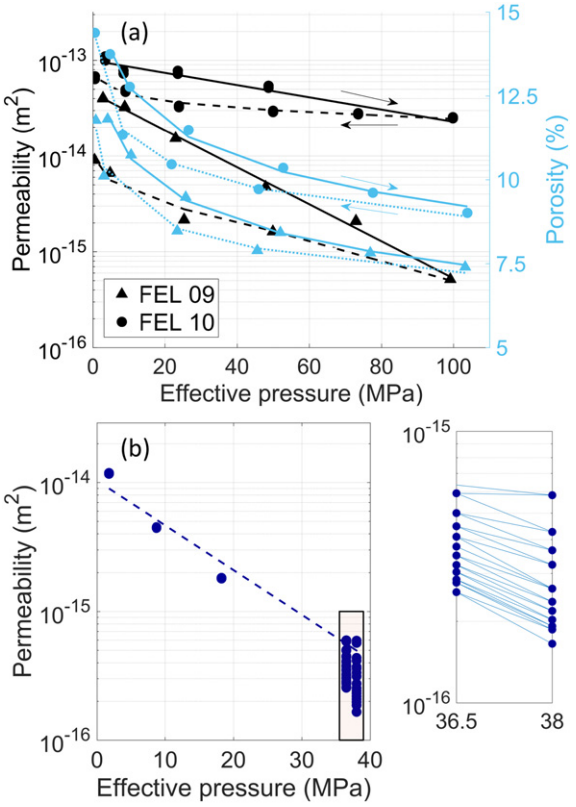

Fig. 6. Variations of: (a) Permeability and porosity of felsite resulting from pore pressure (and thus effective pressure) loading/unloading cycles to 100 MPa. The figure shows a degree of hysteresis; as effective pressure is decreased the sample does not recover the initial (i.e., lower pressure) permeability and porosity of the rock. (b) Permeability evolution of felsite during pore pressure (hence, effective pressure) oscillations of 1.5 MPa. The data (zoomed-in inset in b) shows that each unloading cycle never fully recovers permeability efficiency, and the permeability lowers further with each loading cycle due to further closure of permeable pathways.

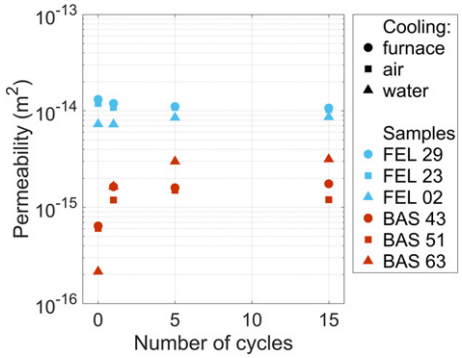

Fig. 7. Influence of thermal stressing (up to 450 °C) cycles on the permeability of basalt (BAS) and felsite (FEL) cooled under different conditions. The data show that the permeability of the felsite is insensitive to thermal fluctuations, presumably as the original sample contains multiple micro-fractures (see Fig. 2). In contrast, the permeability of the basalt non-linearly increases with thermal cycles (especially the first five cycles). We note that permeability is highest in samples cooled by water (triangles), compared to cooling in ambient air or under controlled conditions in the furnace (i.e., at <5 °C·min^{-1}).

3.5. Impact of one macro-fracture

The effect of a macro-fracture on the permeability of a sample has been the focus of recent studies (Heap and Kennedy, 2016; Lamur et al., 2017a; Nara et al., 2011); here we expand this dataset by testing the impact of macro-fractures on several lithologies. Of the lithologies tested here, the hyaloclastite did not withstand a fracture, but rather compacted during Brazilian tensile testing, and therefore the permeability of fractured hyaloclastite could not be measured. Similarly, of the felsite cores tested, only a few developed clean fractures during mechanical testing, therefore reducing the number of fractured samples measured for permeability. The basaltic dyke was not subjected to this testing method (as we had insufficient material).

For the dense basalt and felsite, for which intact samples showed a wide range of permeabilities, the presence of a fracture narrowed the range of permeabilities to relatively high values (Fig. 8a, c). In contrast, the permeability of the porous basalt was not affected by the addition of a macro-fracture (Fig. 8b). For all other samples, imparting a fracture increased permeability by as much as 2–5 orders of magnitude (Fig. 8d–f).

Effective pressure showed variable influences on the permeability (Fig. 5) of these macro-fractured rocks; yet, permeability decrease was generally greatest in the early stages of confinement, and for most samples led to a nonlinear decrease of 1–2 orders of magnitude of permeability (Figs. 8 and 9). The sensitivity of permeability of fractured samples to confinement was heightened as compared to their intact counterparts (Figs. 5 and 8). Within one lithology (basalt) however, the sensitivity to confinement was variable (Fig. 9); yet, these macro-fractures are irregular, and bordered by minor fractures and fragments (Fig. 10).

Table 1
Porosity of volcanic rocks subjected to thermal stressing cycles.

	Porosity (%)			
Number of cycles	0	1	5	15
FEL_TRI_29	10.3	10.5	10.3	10.5
FEL_TRI_23	9.4	9.3	9.4	9.3
FEL_PP_02	9.8	9.8	9.9	9.9
BAS_TRI_43	11.5	11.5	11.4	11.4
BAS_TRI_51	12.1	12.2	12.1	12.0
BAS_TRI_63	10.9	11.1	10.9	11.1

3.6. Impact of two macro-fractures

The basalts, being a key rock type in Iceland and the most mechanically consistent rock of the lithologies at Krafla, were used to test the impact of two orthogonal macro-fractures on the permeable porous network, as they display a wide range of initial porosities and permeabilities. The tests were systematically conducted on six samples, ranging between 10.9 and 21.3 vol% porosity.

The generation of a second, orthogonal fracture increased the permeability of the rocks further for samples across the range of porosities tested. The most porous sample (Fig. 9f) was unable to sustain the fracture and crumbled. The permeability increase induced by the second fracture was not as significant as the first fracture (Figs. 8–9), despite creating more fracture surface area and increasing porosity. This observation remains valid over the range of effective pressures tested; the interesting exception to this is the sample with 13.5% porosity, for which the second fracture seems not to close adequately with an increase in effective pressure, resulting in a permeability nearly an order of magnitude higher than the single-fractured sample at 100 MPa effective pressure. For all other samples with 1 or 2 fractures, upon confinement, the permeability trends towards that of the intact rock. This convergence is not always possible, and appears less readily attainable in the lower porosity samples (Fig. 9a–c), which have the lowest initial permeability values and for which the permeability is most affected by fracturing.

4. Discussion and implications

The findings presented here enhance our understanding of the impacts of thermal and mechanical stimulation practices. The data shows

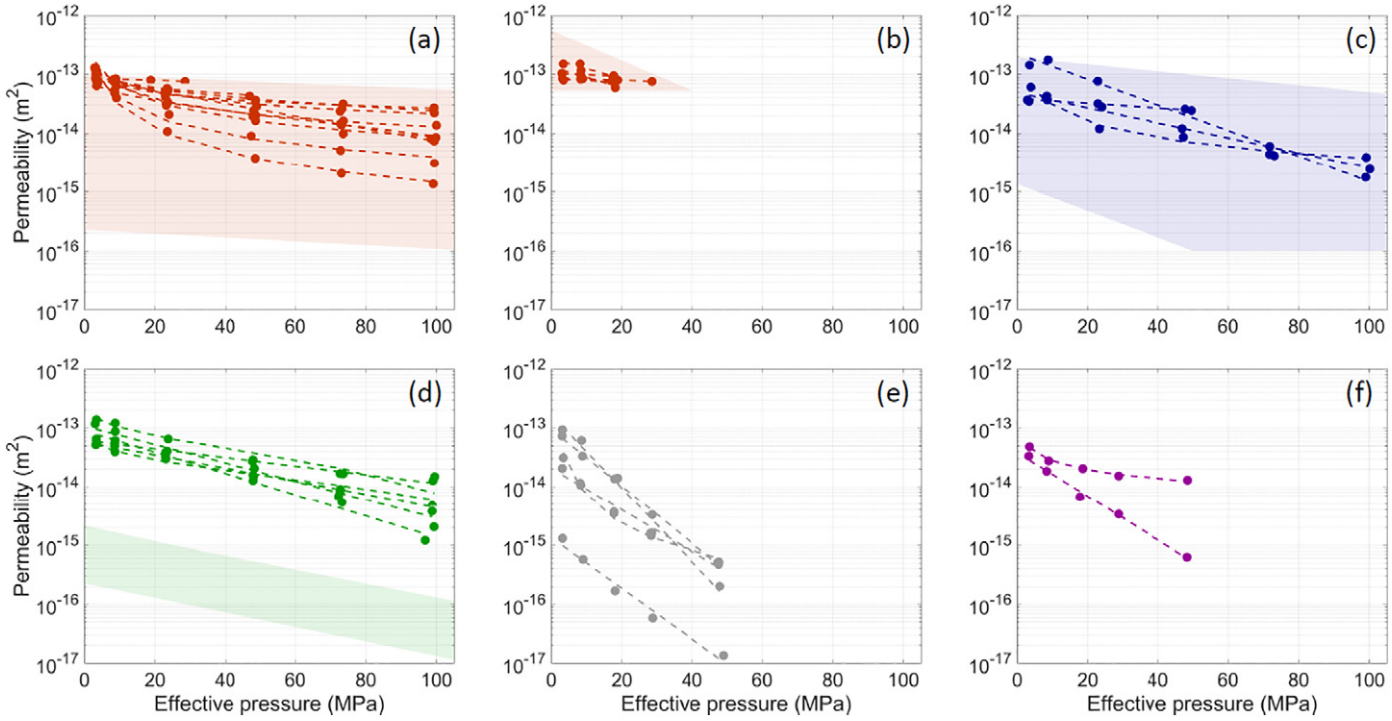

Fig. 8. Permeability evolution with effective pressure of macro-fractured (a) dense basalt (10 samples), (b) porous basalt (5 samples), (c) felsite (4 samples), (d) gabbro (6 samples tested), (e) Ignimbrite (5 samples), and (f) obsidian (2 samples). The shaded areas show the range of permeability of intact samples before they were fractured (from Fig. 5), showing the variable effect of fractures on permeability. Note that the permeability of the intact ignimbrite and obsidian was below the detection limit for our apparatus (which was developed for permeable samples).

that pore pressure fluctuations at pressures lower than the local confining pressure may not be an effective way to increase the permeability of a reservoir; yet, we surmise that if this pore pressure variation takes place at pressures nearing or exceeding the local stress – a condition favouring tensile fracture propagation (see Section 4.1), then the effect may be quite contrasting (e.g. Rozhko et al., 2007). Thermal stimulation demonstrated variable influence on the resultant permeable porous network. Here, we noted that rocks void of micro-fractures were more

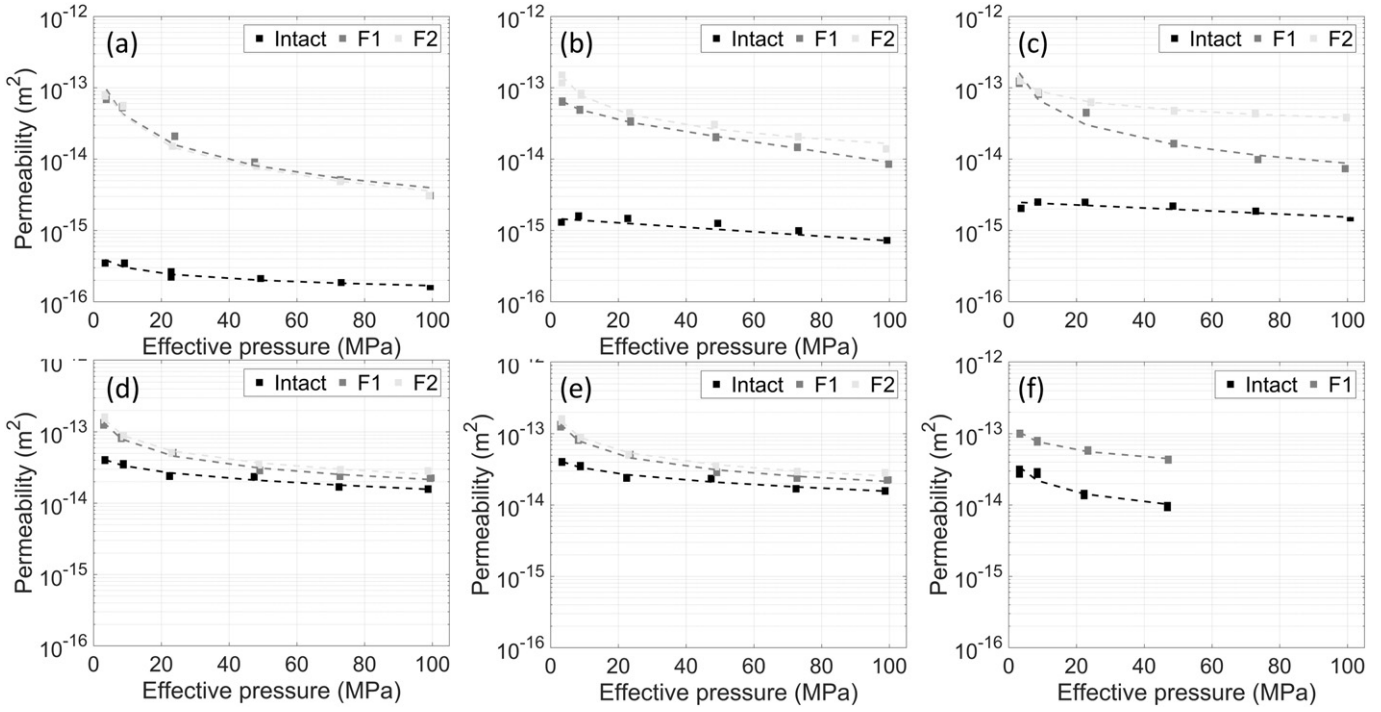

Fig. 9. Permeability variations with effective pressure for intact samples, and the same samples with one fracture (F1) and two fractures (F2), imparted experimentally for basalts with a range of initial porosities from (a) 10.9%, (b) 12.9%, (c) 13.5%, (d) 14.8%, (e) 15.9% to (f) 21.3%.The data show a 0.5 to >2 order of magnitude increase in permeability due to fracturing, which is more significant at low porosity. Increasing effective pressure closes the fracture and the permeability nonlinearly decreases, trending towards that of the intact rock. This convergence is not always possible, presumably as in imperfect contact or dislodged fragments may obstruct fracture closure (See Fig. 10).

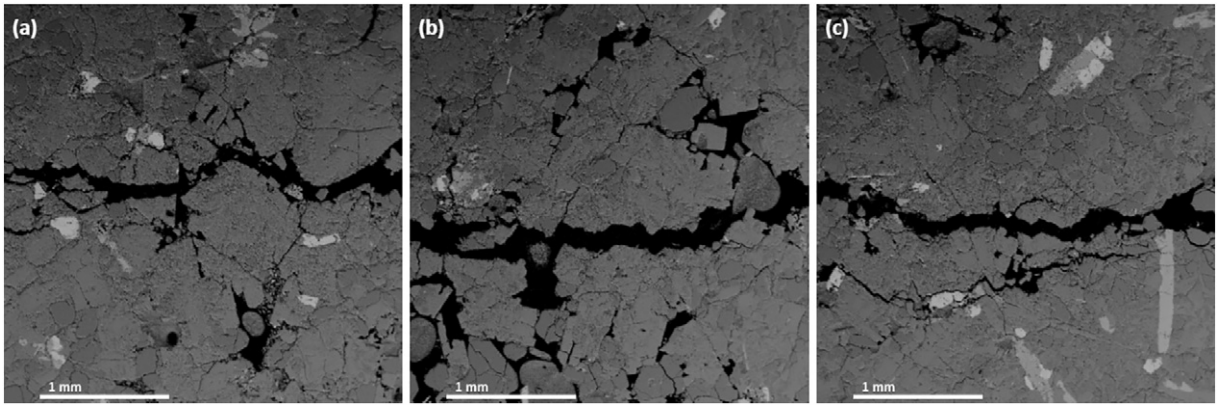

Fig. 10. Backscattered electron (BSE) images (obtained by scanning electron microscope (SEM)) of fractures generated in the felsite (average 11.5% porosity). The images show that failure was accommodated by a macro-fracture, hosting small rock fragments and bordered by fine, branching subparallel fractures, with slight variability within one lithology.

liable to thermal stressing than micro-fractured rocks. This may be because, when present in a rock, micro-fractures may simply open during cooling contraction of the solid phase, without building large tensile stresses; in contrast, crack-poor rocks would build up large tensile stresses during cooling contraction, which may result in cracking, and thus enhanced fluid flow. The observed change in permeability of about one order of magnitude is moderate compared to Siratovich et al. (2015a), which showed a permeability change by three orders of magnitude for the dense andesite of the Rotokawa geothermal field. Thus, the permeability of hydrothermal reservoirs may be subject to changes in the lifetime of fluid extraction if it results in temperature changes, especially if rapidly heating and cooling dense unfractured lithologies. Yet ultimately, it is the generation of fractures, whether microscopic or macroscopic in nature, which controls permeability in the reservoirs, and arguably when fractures are mechanically impeded from adequate closure that they present the most persistent fluid pathways.

4.1. On the permeability of intact and fractured volcanic rocks

Detailed knowledge of the storage capacity and permeability of reservoir rocks is crucial to improve the utilisation of geothermal resources and to maximise energy production. The experimental work carried out here sheds light on the efficiency of fluid flow through the permeable porous network in the Krafla geothermal reservoir. The reservoir consists of a succession of mafic lavas, ignimbrites and hyaloclastites at shallow depth (<1 km) and at greater depth (>1 km), of cross-cutting mafic, intermediate and felsic intrusions (Mortensen et al., 2015). All the rocks display a range of porosities and permeabilities, and correspondingly, differing responses to effective pressure. The rocks found at shallow depths are highly variable: the basaltic rocks have a wide range of porosities and permeabilities, and the densest lithologies remain strong when pressurised (or, in natural terms, buried); whereas the porous basalt and hyaloclastite can only experience relatively low confinement without undergoing compaction (at P*). The intrusive rocks originating at depth were observed to be highly fractured, which led to high permeability (and higher dependence of permeability on effective pressure), despite their low porosities. The basaltic dyke however has low permeability, despite relatively high porosity (32–34 vol % porosity; Fig. 11), due to a predominantly isolated pore structure (Fig. 2c). Within the reservoir, we expect that other dykes may be denser and less permeable.

When compiled together, the permeability of the intact rocks increases non-linearly with porosity (Fig. 11), as previously described (e.g. Ashwell et al., 2015; Brace, 1980; Eichelberger et al., 1986; Farquharson et al., 2015; Heap et al., 2014a; Heap and Kennedy, 2016; Heap et al., 2014b; Heap et al., 2016; Jouniaux et al., 2000; Kendrick et al., 2016; Kendrick et al., 2013; Klug and Cashman, 1996; Kushnir et al., 2016; Lamur et al., 2017a; Mueller et al., 2005; Okumura and Sasaki, 2014; Saar and Manga, 1999; Schaefer et al., 2015; Stimac et al., 2004). [It should be noted that previously published data collected at slightly different effective pressures (e.g. Tanikawa and Shimamoto, 2009) may increase scatter.] As permeability-porosity measurements of a variety of volcanic rocks accrue (e.g. Farquharson et al., 2015; Lamur et al., 2017a; Mueller et al., 2005), a picture is rapidly emerging which depicts a wide range of permeabilities at all porosities (e.g., at ~10% and ~35% in Fig. 11); here, we advance that the absence of a petrogenetic link between rocks with different porosities and permeabilities (owing to distinct petrological and deformational histories) may preclude the necessity to invoke a change point dividing two permeability regimes – fracture- vs vesicle-controlled – (even if statistically determined by the current dataset) and that a simple power-law regression may be an equally adequate approximation to be used in simulations, until a genetic link is established.

The addition of a macro-fracture increases the permeability of porous volcanic rocks. Recent experimental investigations (Heap and Kennedy, 2016; Lamur et al., 2017a) have proposed models to constrain the impact of fractures on permeability as a function of effective pressure, demonstrating that in the presence of one fracture, the permeability-porosity relationship follows a power law dependence (Lamur et al., 2017a); here, our dataset appears to abide to such a power-law relationship (Fig. 12). The permeability-porosity relationship of fractured volcanics further appears to limit the permeability of all porous rocks (>15 vol% porosity) present at Krafla (Fig. 11).

The data presented here further suggest that the obstruction of fractures by particles locally fragmented and offset between fracture planes may prevent complete fracture closure (Fig. 10). This influence is more likely as more fractures are introduced, and results in persistence of high permeability even at high effective pressures. Perez-Flores et al. (2017) showed that the effect of fracture offset on permeability varies between lithologies, but at a certain offset length, the effect on permeability reached a maximum, which for fresh basalt, was around two orders of magnitude of permeability. With time, offset fractures also withhold a higher permeability, by keeping the fracture network open even if pressure changes (Hofmann et al., 2016), as we observe. Fracture closure and fracture network repsonse to changes in effective pressure have also been shown to be controlled by the mechanical properties of a rock type, as stronger rocks may prevent efficient fracture closure, whereas weak rocks may deform and shut fractures (Milsch et al., 2016). Slurries containing sand particles (proppants) with the purpose of obstructing fracture closure have been used to optimise reservoir permeability and fluid extraction (Brinton et al., 2011), and our findings corroborate these practices. We further suggest that strategic thermo-mechanical stressing to impart fractures which orthogonally intersect local or regional fractures may be an equally efficient way to increase the permeability of a reservoir and thus, its resultant energy output.

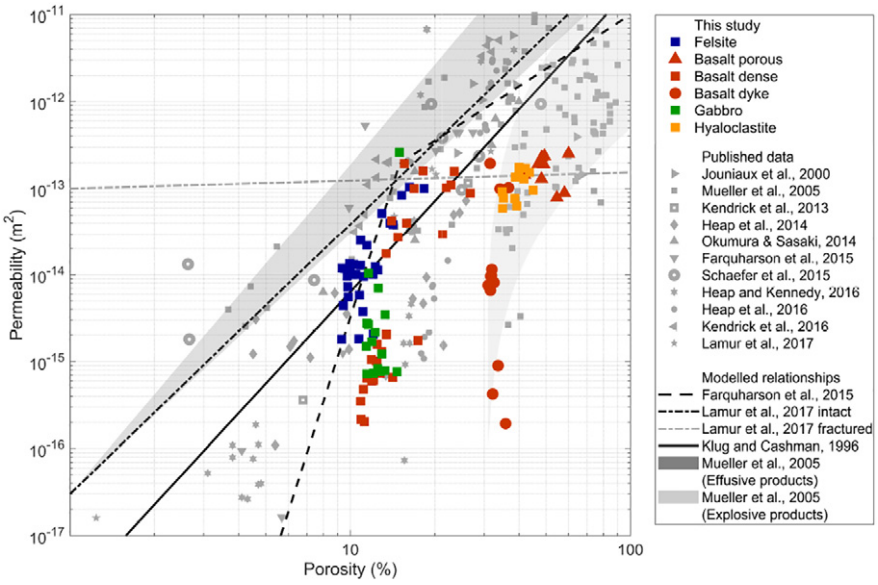

Fig. 11. Permeability (measured at P_{eff} = 3,75 MPa) as a function of porosity, showing the extensive variability of the lithologies examined. Data from this study correlate well with previously published data (measured at a range of effective pressures, which increases scatter further). Comparing the data to models to describe the porosity-permeability relationship, we note that the model for explosive products from Mueller et al. (2005) correlates very well with samples collected form a dyke. For the lower porosity samples, the model proposed by Farquharson et al. (2015) shows a better correlation than other models proposed, with a rapid increase in permeability over relatively narrow range of porosity, although above the inflection point the trend does not correlate well. Rather, it appears that the relationship for fractured rocks from Lamur et al. (2017a) appropriately describes the upper limit of permeability observed here.

The outcome of this practice may likely be enhanced if the fracture produced is strategically aligned at low angles to the principal stress (in an anisotropic stress field) to favour slight displacement/misalignment of the fracture interfaces, which may leave gaps in the rock to permit extensive fluid flow. This effect may be central to the efficiency of thermo-mechanically derived fractures as pathways to increase connectivity in the reservoir.

4.2. Permeability of the Krafla hydrothermal reservoir

Today at Krafla, geothermal energy production focuses on fluid extraction at shallow depth up to about 2–3 km (Mortensen et al., 2015); yet, deeper fluid extraction is often contemplated in our pursuit of higher energy production (Fridleifsson et al., 2014). In doing so, efforts must be made to avoid intersecting the shallow magma reservoir located at a depth of 2.1 km (Elders et al., 2014). Geochemical investigation of the glass fragments recovered during drilling into the magma reservoir suggests that volatile concentration is in equilibrium with a temperature of 800–950 °C (Axelsson et al., 2014; Elders et al., 2011) and a pressure of 30–50 MPa (Elders et al., 2011). At Krafla, a depth of 2.1 km corresponds to a lithostatic pressure of approximately 65 MPa, if we assume a rock density of 3100 kg/m^3 for the predominantly basaltic chemistry of these volcanics; thus, the discrepancy between the estimated equilibrium and the approximation of the lithostatic load suggests that fluid connectivity in the hydrothermal system may be efficiently decrease local magmatic pressure to below lithostatic. Thus, we can assume that at any given depth in the Krafla hydrothermal reservoir, the effective pressure can be approximated by subtracting the hydrostatic pressure (i.e., the pore pressure in our experiments) from the lithostatic pressure (i.e., the confining pressure in our experiments). Therefore, a depth of 2–3 km may correspond to effective pressures of 40–50 MPa (in agreement with equilibrium conditions for the glass; Elders et al., 2011). The study shows that the storage capacity and permeability of the reservoir rocks nonlinearly increases by decreasing the effective pressure exerted in the system, so fluid extraction may be optimised by ensuring high pressure of fluid injected into the hydrothermal system to keep fractures open as wide as permits (whilst remaining stable and not creating undesired hydraulic fractures).

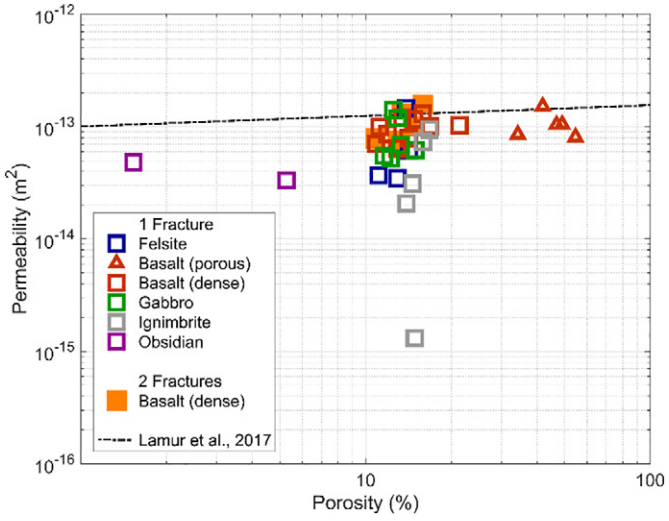

Fig. 12. The connected porous network of the fractured samples shows a very narrow variability of permeability across all lithologies, typically <1 order of magnitude (P_{eff} = 3.75 MPa) across a wide range of starting porosities. The data is compared to the relationship for fractured rock permeability described in Lamur et al. (2017a) for the correct effective pressure. This relationship appropriately to describe the dataset with both 1 and 2 macrofractures, as well as appearing to describe the upper permeability limit of our intact samples (Fig. 11).

During IDDP-1, drilling activities suffered from a loss in fluids shortly before intersecting the magma reservoir at 2.1 km (Palsson et al., 2014). This 50-m thick zone of fluid loss coincided with encountering felsite – a crystalline rock believed to represent the crystallised aureole that surrounds the magma reservoir (Mortensen et al., 2014). No large samples of felsite were retrieved by the drilling activities, but samples can be collected from the phreatomagmatic deposits that surround the Viti crater (Sæmundsson, 1991). In this study, we examined gabbro and felsite blocks from this phreatomagmatic event and we found that both samples are highly micro-fractured (Fig. 2d, e), which results in high permeability (and fracture compressibility with effective pressure). Phreatomagmatic eruptions are known to be highly explosive (Austin-

Erickson et al., 2008) and we postulate that the high fracture density observed in the samples tested here is congruent with their eruption and with a damaged source region due to thermal jointing during magma cooling (e.g., Lamur et al., 2018). Deep-seated fragmentation at depths of ca. 2.1 km, perhaps even due to emplacement of the rhyolitic magma, may thus be at the origin of this felsitic zone with high-fracture density that led to important fluid loss during IDDP-1. If such is the case, the high permeability of fractured magmatic aureoles – commonly believed not to have open fractures due to their propensity to flow and heal (e.g. Scott et al., 2015) – may be key in ensuring fluid connectivity between the Earth's surface and the magma reservoir (e.g., Lamur et al., 2018). This permeable architecture may naturally prevent from the accumulation of excess volatile concentration, dissolved in the magma, making it not particularly buoyant and hence unlikely to erupt during drilling operations.

The laboratory measurements performed on samples primarily collected from surficial outcrops at Krafla, offer a first order constraint on the storage capacity and permeability of the reservoir rock present at Krafla volcano. Yet, much remains to be investigated to obtain a complete picture of fluid flow in this hydrothermal system: from complexity arising from the effects of high-temperatures (Kushnir et al., 2017a; Violay et al., 2017) to the influence exerted by devolatilisation (e.g. Heap et al., 2013), dissolution (Gislason and Arnorsson, 1993), clogging by fine fragments (e.g. Farquharson et al., 2017; Kendrick et al., 2016) and secondary mineral precipitation (e.g. Curewitz and Karson, 1997). Such descriptions are the subject of ongoing work as part of the international IDDP and KMT projects.

5. Conclusions

This experimental study describes the permeability and storage capacity of the lithologies found within the Krafla reservoir. We find that each lithology exhibits a wide range of porosity and permeability; both of which are found to decrease nonlinearly with effective pressure – an effect which is more pronounced in samples with significant presence of fractures. We tested the influence of pressure oscillations, thermal stressing and fracturing on fluid flow in these rocks. We found that pressurisation/depressurisation cycles leads to the progressive shutting of micro-fractures, which result in an overall permeability decrease of the rocks, though our experiments fluctuated pore pressure at values significantly lower than confinement, and we postulate that the effect may be reversed if pore pressure locally exceeded confining pressure. Thermal stimulation (especially when thermal shocks are caused by water) results in an increase of the permeability of rocks which are originally devoid of significant micro-fractures; however, fractured rocks remain largely unaffected by thermal stressing. Imparting a single macro-fracture increases the permeability of a rock at low effective pressure, but as confinement increases, the fracture begins to close and permeability trends towards that of the intact rock; imparting a second orthogonal fracture offers only a slightly higher increase in permeability of the rocks, but increases the possibility of offset along the fractures and thus the persistence of high permeability under confinement. Where the fracture was slightly offset, or where fine fragments lodged themselves in the fracture, obstruction from closure at high effective pressure resulted in high, relatively pressure-independent permeabilities. The data suggests that when thermo-mechanically stimulating a reservoir, efforts should be made to generate fractures orthogonal to primary local faults and fractures, or at low angle to principal stresses in order to increase gap opening at their intersections and favour fluid flow in the hydrothermal system. These findings support the use of proppants, such as non-reactive granular materials, to open fractures and ensure efficient fluid flow in production wells.

Supplementary data to this article can be found online at https://doi.org/10.1016/j.jvolgeores.2018.04.008.

Acknowledgements

This study has been partially financed by research funds from Landsvirkjun (grant nos. NÝR-17-2015, NÝR-15-2016, NÝR-20-2017) National Power Company of Iceland as well as a scholarship from the Institute for Risk and Uncertainty at the University of Liverpool and the European Research Council Starting Grant on Strain Localisation in Magma (SLiM, no. 306488). We wish to thank Dr. M.J. Heap and an anonymous reviewer for constructive comments as well as A. Lamur for fruitful discussions.

References

Alam, A.K.M.B., Niioka, M., Fujii, Y., Fukuda, D., Kodama, J.-i., 2014. Effects of confining pressure on the permeability of three rock types under compression. Int. J. Rock Mech. Min. Sci. 65, 49–61.
Aqui, A.R., Zarrouk, S., 2011. Permeability Enhancement of Conventional Geothermal Wells. New Zealand Geothermal Workshop, Auckland, New Zealand.
Ármannsson, H., 1989. Gas changes in the Krafla geothermal system, Iceland. Water-Rock Interact. 76 (3–4), 19.
Ashwell, P.A., Kendrick, J.E., Lavallée, Y., Kennedy, B.M., Hess, K.U., von Aulock, F.W., Wadsworth, F.B., Vasseur, J., Dingwell, D.B., 2015. Permeability of compacting porous lavas. J. Geophys. Res. Solid Earth 120 (3), 2014JB011519.
Austin-Erickson, A., Buttner, R., Dellino, P., Ort, M.H., Zimanowski, B., 2008. Phreatomagmatic explosions of rhyolitic magma: Experimental and field evidence. J. Geophys. Res. Solid Earth 113 (B11).
Axelsson, G., Egilson, T., Gylfadottir, S.S., 2014. Modelling of temperature conditions near the bottom of well IDDP-1 in Krafla, Northeast Iceland. Geothermics 49, 49–57.
Bodvarsson, G.S., Pruess, K., Stefansson, V., Eliasson, E.T., 1984. The krafla geothermal field, Iceland: 2. Nat. State Syst. Water Resour. Res. 20 (11), 14.
Brace, W.F., 1980. Permeability of crystalline and argillaceous rocks. Int. J. Rock Mech. Min. Sci. 17 (5), 241–251.
Brace, W.F., Walsh, J.B., Frangos, W.T., 1968. Permeability of granite under high pressure. J. Geophys. Res. 73 (6), 2225–2236.
Brinton, D., McLin, K., Moore, J., 2011. The Chemical Stability of Bauxite and Quartz Sand Proppants Under Geothermal Conditions, 36th Stanford Geothermal Workshop on Geothermal Reservoir Engineering. California, Stanford.
Cant, J.L., Siratovich, P.A., Cole, J.W., Villeneuve, M.C., Kennedy, B.M., 2018. Matrix permeability of reservoir rocks, Ngatamariki geothermal field, Taupo Volcanic Zone, New Zealand. Geotherm. Energy 6 (2).
Carlino, S., Somma, R., Troise, C., De Natale, G., 2012. The geothermal exploration of Campanian volcanoes: historical review and future development. Renew. Sust. Energ. Rev. 16 (1), 1004–1030.
Curewitz, D., Karson, J.A., 1997. Structural settings of hydrothermal outflow: fracture permeability maintained by fault propagation and interaction. J. Volcanol. Geotherm. Res. 79 (3–4), 149–168.
Darcy, H., 1856. Les fontaines publiques de la ville de Dijon. Dalmont, Paris.
Darcy, H., 1857. Recherches expérimentales relatives au mouvement de l'eau dans les tuyaux. Mallet-Bachelier, École impériale polytechnique de Paris.
Darling, W.G., Armannsson, H., 1989. Stable isotopic aspects of fluid-flow in the Krafla, Namafjall and Theistareykir geothermal systems of Northeast Iceland. Chem. Geol. 76 (3–4), 197–213.
Degraff, J.M., Aydin, A., 1993. Effect of thermal regime on growth increment and spacing of contraction joints in basaltic lava. J. Geophys. Res. Solid Earth 98 (B4), 6411–6430.
Edmonds, M., Herd, R.A., 2007. A volcanic degassing event at the explosive-effusive transition. Geophys. Res. Lett. 34 (21), L21310.
Eggertsson, G.H., Lavallée, Y., Kendrick, J.E., Lamur, A., Markússon, S., 2016. Enhancing Permeability by Multiple Fractures in the Krafla Geothermal Reservoir, Iceland, European Geothermal Congress. European Geothermal Congress, Strasbourg.
Eichelberger, J.C., Carrigan, C.R., Westrich, H.R., Price, R.H., 1986. Non-explosive silicic volcanism. Nature 323 (6089), 598–602.
Einarsson, P., 1978. S-wave shadows in the Krafla caldera in NE Iceland: evidence for a magma chamber in the crust. Bull. Volcanol. 41 (3), 8.
Einarsson, P., 1991. The Krafla rifting episode 1975–1989 (Umbrotin við Kröflu 1975–89 in Icelandic). Hið íslenska náttúrufræðifélag, Reykjavík (43 pp).
Elders, W.A., Frioleifsson, G.O., Zierenberg, R.A., Pope, E.C., Mortensen, A.K., Guomundsson, A., Lowenstern, J.B., Marks, N.E., Owens, L., Bird, D.K., Reed, M., Olsen, N.J., Schiffman, P., 2011. Origin of a rhyolite that intruded a geothermal well while drilling at the Krafla volcano, Iceland. Geology 39 (3), 231–234.
Elders, W.A., Fridleifsson, G.O., Palsson, B., 2014. Iceland Deep Drilling Project: the first well, IDDP-1, drilled into magma Preface. Geothermics 49, 1.
Farquharson, J., Heap, M.J., Varley, N.R., Baud, P., Reuschle, T., 2015. Permeability and porosity relationships of edifice-forming andesites: a combined field and laboratory study. J. Volcanol. Geotherm. Res. 297, 52–68.
Farquharson, J.I., Wadsworth, F.B., Heap, M.J., Baud, P., 2017. Time-dependent permeability evolution in compacting volcanic fracture systems and implications for gas overpressure. J. Volcanol. Geotherm. Res. 339, 81–97.
Fournier, R.O., 1999. Hydrothermal processes related to movement of fluid from plastic into brittle rock in the magmatic-epithermal environment. Econ. Geol. Bull. Soc. Econ. Geol. 94 (8), 1193–1211.
Fridleifsson, G.O., Elders, W.A., Albertsson, A., 2014. The concept of the Iceland deep drilling project. Geothermics 49, 2–8.

Gallois, R., 2007. The formation of the hot springs at Bath Spa, UK. Geol. Mag. 144 (4), 741–747.

Ghassemi, A., 2012. A review of some rock mechanics issues in geothermal reservoir development. Geotech. Geol. Eng. 30 (3), 647–664.

Gislason, S.R., Arnorsson, S., 1993. Dissolution of primary basaltic minerals in natural waters: saturation state and kinetics. Chem. Geol. 105 (1–3), 117–135.

Grant, M.A., Clearwater, J., Quinão, J., Bixley, P.F., Le Brun, M., 2013. Thermal Stimulation of Geothermal Wells: A Review of Field Data, Proceedings.

Gudmundsson, A., 1995. Infrastructure and mecahnics of volcanic systems in Iceland. J. Volcanol. Geotherm. Res. 64 (1–2), 1–22.

Guðmundsson, Á., 2001. An expansion of the Krafla Power Plant from 30 to 60 MW_e - Geothermal considerations. Geotherm. Resour. Counc. Trans. 25, 6.

Gudmundsson, M.T., Larsen, G., Hoskuldsson, A., Gylfason, A.G., 2008. Volcanic hazards in Iceland. Jökull 58, 251–268.

Hansell, A., Oppenheimer, C., 2004. Health hazards from volcanic gases: a systematic literature review. Arch. Environ. Health 59 (12), 628–639.

Heap, M.J., Kennedy, B.M., 2016. Exploring the scale-dependent permeability of fractured andesite. Earth Planet. Sci. Lett. 447, 139–150.

Heap, M.J., Mollo, S., Vinciguerra, S., Lavallée, Y., Hess, K.U., Dingwell, D.B., Baud, P., Iezzi, G., 2013. Thermal weakening of the carbonate basement under Mt. Etna volcano (Italy): Implications for volcano instability. J. Volcanol. Geotherm. Res. 250, 42–60.

Heap, M., Xu, T., Chen, C.-f., 2014a. The influence of porosity and vesicle size on the brittle strength of volcanic rocks and magma. Bull. Volcanol. 76 (9), 1–15.

Heap, M.J., Kolzenburg, S., Russell, J.K., Campbell, M.E., Welles, J., Farquharson, J.I., Ryan, A., 2014b. Conditions and timescales for welding block-and-ash flow deposits. J. Volcanol. Geotherm. Res. 289, 202–209.

Heap, M.J., Farquharson, J.I., Baud, P., Lavallee, Y., Reuschle, T., 2015a. Fracture and compaction of andesite in a volcanic edifice. Bull. Volcanol. 77 (6).

Heap, M.J., Kennedy, B.M., Pernin, N., Jacquemard, L., Baud, P., Farquharson, J.I., Scheu, B., Lavallee, Y., Gilg, H.A., Letham-Brake, M., Mayer, K., Jolly, A.D., Reuschle, T., Dingwell, D.B., 2015b. Mechanical behaviour and failure modes in the Whakaari (White Island volcano) hydrothermal system, New Zealand. J. Volcanol. Geotherm. Res. 295, 26–42.

Heap, M.J., Russell, J.K., Kennedy, L.A., 2016. Mechanical behaviour of dacite from Mount St. Helens (USA): a link between porosity and lava dome extrusion mechanism (dome or spine)? J. Volcanol. Geotherm. Res. 328, 159–177.

Hjartardottir, A.R., Einarsson, P., Bramham, E., Wright, T.J., 2012. The Krafla fissure swarm, Iceland, and its formation by rifting events. Bull. Volcanol. 74 (9), 2139–2153.

Hofmann, H., Blocher, G., Milsch, H., Babadagli, T., Zimmermann, G., 2016. Transmissivity of aligned and displaced tensile fractures in granitic rocks during cyclic loading. Int. J. Rock Mech. Min. Sci. 87, 69–84.

Ingason, K., Kristjansson, V., Einarsson, K., 2014. Design and development of the discharge system of IDDP-1. Geothermics 49, 58–65.

Jansen, J.D., 2011. Adjoint-based optimization of multi-phase flow through porous media - a review. Comput. Fluids 46 (1), 40–51.

Jouniaux, L., Bernard, M.L., Zamora, M., Pozzi, J.P., 2000. Streaming potential in volcanic rocks from Mount Pelee. J. Geophys. Res. Solid Earth 105 (B4), 8391–8401.

Kantha, L.H., 1981. Basalt fingers - origin of columnar joints. Geol. Mag. 118 (3), 251.

Kendrick, J.E., Lavallée, Y., Hess, K.U., Heap, M.J., Gaunt, H.E., Meredith, P.G., Dingwell, D.B., 2013. Tracking the permeable porous network during strain-dependent magmatic flow. J. Volcanol. Geotherm. Res. 260, 117–126.

Kendrick, J.E., Lavallee, Y., Varley, N.R., Wadsworth, F.B., Lamb, O.D., Vasseur, J., 2016. Blowing off steam: tuffisite formation as a regulator for lava dome eruptions. Front. Earth Sci. 4.

Klug, C., Cashman, K.V., 1996. Permeability development in vesiculating magmas: implications for fragmentation. Bull. Volcanol. 58 (2–3), 87–100.

Kolzenburg, S., Heap, M.J., Lavallée, Y., Russell, J.K., Meredith, P.G., Dingwell, D.B., 2012. Strength and permeability recovery of tuffisite-bearing andesite. Solid Earth 3 (2), 191–198.

Koudina, N., Garcia, R.G., Thovert, J.F., Adler, P.M., 1998. Permeability of three-dimensional fracture networks. Phys. Rev. E 57 (4), 4466–4479.

Kushnir, A.R.L., Martel, C., Bourdier, J.-L., Heap, M.J., Reuschlé, T., Erdmann, S., Komorowski, J.-C., Cholik, N., 2016. Probing permeability and microstructure: unravelling the role of a low-permeability dome on the explosivity of Merapi (Indonesia). J. Volcanol. Geotherm. Res. 316, 56–71.

Kushnir, A.R.L., Martel, C., Champallier, R., Wadsworth, F.B., 2017a. Permeability evolution in variably glassy basaltic andesites measured under magmatic conditions. Geophys. Res. Lett. 44 (20), 10262–10271.

Kushnir, A.R.L., Martel, C., Champallier, R., Wadsworth, F.B., 2017b. Permeability evolution in variably glassy basaltic andesites measured under magmatic conditions. Geophys. Res. Lett. 44, 10, 262–10, 271.

Lamur, A., Kendrick, J.E., Eggertsson, G.H., Wall, R.J., Ashworth, J.D., Lavallee, Y., 2017a. The permeability of fractured rocks in pressurised volcanic and geothermal systems. Sci. Rep. 7.

Lamur, A., Kendrick, J.E., Eggertsson, G.H., Wadsworth, F.B., Ashworth, J.D., Wall, R.J., von Aulock, F.W., Lavallée, Y., 2017b. Fracture, heal, repeat: Timescales and implications for silicic systems' eruptive behaviour. International Association of Volcanology and Chemistry of the Earth's Interior (IAVCEI) conference proceeding.

Lamur, A., Lavallée, Y., Iddon, F., Hornby, A.J., Kendrick, J.E., von Aulock, F.W., Wadsworth, F.B., 2018. Disclosing the temperature of columnar jointing and fluid flow in lavas. Nat. Commun. 9, 1432.

Lavallée, Y., Meredith, P.G., Dingwell, D.B., Hess, K.U., Wassermann, J., Cordonnier, B., Gerik, A., Kruhl, J.H., 2008. Seismogenic lavas and explosive eruption forecasting. Nature 453 (7194), 507–510.

Lavallée, Y., Benson, P.M., Heap, M.J., Hess, K.U., Flaws, A., Schillinger, B., Meredith, P.G., Dingwell, D.B., 2013. Reconstructing magma failure and the degassing network of dome-building eruptions. Geology 41.

Legarth, B., Huenges, E., Zimmermann, G., 2005. Hydraulic fracturing in a sedimentary geothermal reservoir: results and implications. Int. J. Rock Mech. Min. Sci. 42 (7–8), 1028–1041.

McClure, M.W., Horne, R.N., 2014. An investigation of stimulation mechanisms in Enhanced Geothermal Systems. Int. J. Rock Mech. Min. Sci. 72, 242–260.

Miller, S.A., 2015. Modeling enhanced geothermal systems and the essential nature of large-scale changes in permeability at the onset of slip. Geofluids 15 (1–2), 338–349.

Milsch, H., Hofmann, H., Blocher, G., 2016. An experimental and numerical evaluation of continuous fracture permeability measurements during effective pressure cycles. Int. J. Rock Mech. Min. Sci. 89, 109–115.

Mock, J.E., Tester, J.W., Wright, P.M., 1997. Geothermal energy from the earth: Its potential impact as an environmentally sustainable resource. Annu. Rev. Energy Environ. 22, 305–356.

Mortensen, A.K., Egilson, P., Gautason, B., Arnadottir, S., Gudmundsson, A., 2014. Stratigraphy, alteration mineralogy, permeability and temperature conditions of well IDDP-1, Krafla, NE-Iceland. Geothermics 49, 31–41.

Mortensen, A.K., Guðmundsson, Á., Steingrímsson, B., Sigmundsson, F., Axelsson, G., Ármannsson, H., Björnsson, H., Ágústsson, K., Sæmundsson, K., Ólafsson, M., Karlsdóttir, R., Halldórsdóttir, S., Hauksson, T., 2015. The Krafla Geothermal System Research Summary and Conceptual Model Revision. Landsvirkjun, Reykjavík.

Mueller, S., Melnik, O., Spieler, O., Scheu, B., Dingwell, D.B., 2005. Permeability and degassing of dome lavas undergoing rapid decompression: an experimental determination. Bull. Volcanol. 67 (6), 526–538.

Murphy, H.D., Tester, J.W., Grigsby, C.O., Potter, R.M., 1981. Energy extraction from fractured geothermal reservoirs in low-permeability crystalline rock. J. Geophys. Res. 86 (NB8), 7145–7158.

Nara, Y., Meredith, P.G., Yoneda, T., Kaneko, K., 2011. Influence of macro-fractures and micro-fractures on permeability and elastic wave velocities in basalt at elevated pressure. Tectonophysics 503.

Nara, Y., Morimoto, K., Hiroyoshi, N., Yoneda, T., Kaneko, K., Benson, P.M., 2012. Influence of relative humidity on fracture toughness of rock: implications for subcritical crack growth. Int. J. Solids Struct. 49.

Okumura, S., Sasaki, O., 2014. Permeability reduction of fractured rhyolite in volcanic conduits and its control on eruption cyclicity. Geology 42 (10), 843–846.

Palsson, B., Holmgeirsson, S., Gudmundsson, A., Boasson, H.A., Ingason, K., Sverrisson, H., Thorhallsson, S., 2014. Drilling of the well IDDP-1. Geothermics 49, 23–30.

Pearson, C., 1981. The relationship between microseismicity and high pore pressures during hydraulic stimulation experiments in low permeability granitic-rocks. J. Geophys. Res. 86 (NB9), 7855–7864.

Perez-Flores, P., Wang, G., Mitchell, T.M., Meredith, P.G., Nara, Y., Sarkar, V., Cembrano, J., 2017. The effect of offset on fracture permeability of rocks from the Southern Andes Volcanic Zone, Chile. J. Struct. Geol. 104, 142–158.

Rozhko, A.Y., Podladchikov, Y.Y., Renard, F., 2007. Failure patterns caused by localized rise in pore-fluid overpressure and effective strength of rocks. Geophys. Res. Lett. 34 (22).

Saar, M.O., Manga, M., 1999. Permeability-porosity relationship in vesicular basalts. Geophys. Res. Lett. 26.

Sæmundsson, K., 1991. Geology of the Krafla Volcanic system (Jarðfræði Kröflukerfisins in Icelandic). In: Garðarsson, A., Einarsson, Á. (Eds.), Náttúra Mývatns. Hið íslenska náttúrufræðifélag, Reykjavík, pp. 24–95.

Schaefer, L.N., Kendrick, J.E., Lavallée, Y., Oommen, T., Chigna, G., 2015. Geomechanical rock properties of a basaltic volcano. Front. Earth Sci. 3.

Scott, S., Driesner, T., Weis, P., 2015. Geologic controls on supercritical geothermal resources above magmatic intrusions. Nat. Commun. 6.

Siratovich, P.A., Heap, M.J., Villenueve, M.C., Cole, J.W., Reuschlé, T., 2014. Physical property relationships of the Rotokawa Andesite, a significant geothermal reservoir rock in the Taupo Volcanic Zone, New Zealand. Geotherm. Energy 2 (1), 1–31.

Siratovich, P.A., von Aulock, F.W., L, Y., C, J.W., K, B.M., Ve, M.C., 2015a. Thermoelastic properties of the Rotokawa Andesite: a geothermal reservoir constraint. J. Volcanol. Geotherm. Res. 301.

Siratovich, P.A., Villeneuve, M.C., Cole, J.W., Kennedy, B.M., Begue, F., 2015b. Saturated heating and quenching of three crustal rocks and implications for thermal stimulation of permeability in geothermal reservoirs. Int. J. Rock Mech. Min. Sci. 80, 265–280.

Stimac, J.A., Powell, T.S., Golla, G.U., 2004. Porosity and permeability of the Tiwi geothermal field, Philippines, based on continuous and spot core measurements. Geothermics 33.

Strehlow, K., Gottsmann, J.H., Rust, A.C., 2015. Poroelastic responses of confined aquifers to subsurface strain and their use for volcano monitoring. Solid Earth 6 (4), 1207–1229.

Tanikawa, W., Shimamoto, T., 2009. Comparison of Klinkenberg-corrected gas permeability and water permeability in sedimentary rocks. Int. J. Rock Mech. Min. Sci. 46 (2), 229–238.

Tiwari, G.N., Ghosal, M.K., 2005. Renewable Energy Resources: Basic Principles and Applications. Alpha Science International.

Tomac, I., Gutierrez, M., 2017. Coupled hydro-thermo-mechanical modeling of hydraulic fracturing in quasi-brittle rocks using BPM-DEM. J. Rock Mech. Geotech. Eng. 9 (1), 92–104.

Tuffen, H., Dingwell, D.B., Pinkerton, H., 2003. Repeated fracture and healing of silicic magma generate flow banding and earthquakes? Geology 31 (12), 1089–1092.

Violay, M., Gibert, B., Mainprice, D., Evans, B., Dautria, J.-M., Azais, P., Pezard, P., 2012. An experimental study of the brittle-ductile transition of basalt at oceanic crust pressure and temperature conditions. J. Geophys. Res. 117.

Violay, M., Heap, M.J., Acosta, M., Madonna, C., 2017. Porosity evolution at the brittle-ductile transition in the continental crust: implications for deep hydro-geothermal circulation. Sci. Rep. 7, 10.

Walsh, J.B., 1981. Effect of pore pressure and confining pressure on fracture permeability. Int. J. Rock Mech. Min. Sci. Geomech. Abstr. 18 (5), 429–435.

Wong, T.-f, Baud, P., 2012. The brittle-ductile transition in porous rock: a review. J. Struct. Geol. 44, 25–53.

Zang, A.N., Oye, V., Jousset, P., Deichmann, N., Gritto, R., McGarr, A., Majer, E., Bruhn, D., 2014. Analysis of induced seismicity in geothermal reservoirs - an overview. Geothermics 52, 6–21.

Zhang, J.X., Wong, T.F., Davis, D.M., 1990. Micromechanics of pressure-induced grain crushing in porous rocks. J. Geophys. Res. Solid Earth Planets 95 (B1), 341–352.

Zierenberg, R.A., Schiffman, P., Barfod, G.H., Lesher, C.E., Marks, N.E., Lowenstern, J.B., Mortensen, A.K., Pope, E.C., Bird, D.K., Reed, M.H., Friðleifsson, G.Ó., Elders, W.A., 2013. Composition and origin of rhyolite melt intersected by drilling in the Krafla geothermal field, Iceland. Contrib. Mineral. Petrol. 165 (2), 327–347.

Zimmermann, G., Tischner, T., Legarth, B., Huenges, E., 2009. Pressure-dependent production efficiency of an enhanced geothermal system (egs): stimulation results and implications for hydraulic fracture treatments. Pure Appl. Geophys. 166 (5–7), 1089–1106.

Zimmermann, G., Blocher, G., Reinicke, A., Brandt, W., 2011. Rock specific hydraulic fracturing and matrix acidizing to enhance a geothermal system - Concepts and field results. Tectonophysics 503 (1–2), 146–154.